Microstructure and strength of selectively laser melted AlSi10Mg

Wu, Jing; Wang, Xiqian; Wang, Wei; Attallah, Moataz; Loretto, Michael

DOI:
10.1016/j.actamat.2016.07.012

Document Version
Peer reviewed version

Citation for published version (Harvard):
Wu, J, Wang, X, Wang, W, Attallah, M & Loretto, M 2016, 'Microstructure and strength of selectively laser melted AlSi10Mg', *Acta Materialia*, vol. 117, pp. 311-320. https://doi.org/10.1016/j.actamat.2016.07.012

Microstructure and Strength of Selectively Laser Melted Al10Si0.4Mg

J. Wu*, X.Q. Wang, W. Wang, M.M. Attallah and M.H. Loretto

Metallurgy and Materials, the University of Birmingham, Edgbaston B15 2TT, UK

Abstract

Samples of laser powder bed processed Al-10Si-0.4Mg have been examined using scanning electron microscopy (SEM), transmission electron microscopy (TEM), and scanning TEM so that the complex microstructures of as-fabricated samples could be characterised. In longitudinal sections, columnar Al grains, about 10μm in diameter, dominate the microstructure, but some equiaxed regions are seen. The columnar grains are made up of long cells, about 500nm in width, rather than dendrites, which are separated from adjacent identical orientation long cells and from non-parallel cells at Al grain boundaries, by Al-Si eutectic. There is a substructure on the scale of 300-500nm, of identical orientation "sub-cells" throughout the length of the long cells also separated by regions of the Al-Si eutectic. Microdiffraction is necessary to distinguish between cell boundaries, sub-cell boundaries and grain boundaries. The "cell-like" structures observed in cross section samples are cross sections of these long cells and of the Al-Si eutectic at cell boundaries. Deformed as-fabricated samples have been examined in TEM to assess the role of Si particles within the cells and of the Al-Si-eutectic boundaries on the response of SLMed samples to plastic deformation. In addition in situ compression tests in a TEM have been carried out which show that cell boundaries, sub-cell boundaries and particles within the cells limit dislocation movement during deformation.

Keywords: AlSi alloys; powder processing; diffraction; cells; eutectic; in-situ compression.

* Corresponding author: J. Wu, Tel: +44 7549644941, Email: jxw256@bham.ac.uk

1 Introduction.

Al-Si alloys are used extensively in the automotive and aerospace industries because they are readily cast and because of their combination of high strength and low density [1, 2]. Conventionally cast Al-Si alloys normally contain coarse, acicular silicon as well as Mg-containing precipitates. The large Si-rich precipitates are detrimental to the ductility and need to be refined [3]. Recently selective laser melting (SLM), which has high heating and cooling rates (10^3–10^5 K/s), has been used to refine the microstructure of Al-Si alloy and significantly improved mechanical properties can be obtained [4-8].

Several papers have been published recently describing the microstructures observed in laser-fabricated samples of the same alloy and of similar alloys [6, 9, 10], however the observations and interpretations differ very significantly. Important differences between the interpretation of the microstructures characterised in the present work and several of these recent papers are discussed in the final section of this paper.

The first aim of the present paper is thus to carry out a 3D analysis of the microstructure by examining cross sections and longitudinal sections of laser-built samples using the various imaging modes in TEM (Transmission Electron Microscopy), SEM (Scanning Electron Microscopy) and STEM (Scanning Transmission Electron Microscopy) together with X-ray maps so that the mechanisms giving rise to the formation of the observed microstructures can be understood.

The second aim is to investigate the factors, which influence the strength of laser-fabricated samples. Previous research on SLMed Al-Si alloys has focussed on assessing the importance of processing parameters on the microstructures developed during SLM and on the resultant mechanical properties [6, 7, 11], but the strengthening mechanism has generally not been assessed. Siddique et al. [7] reported the yield strength of a SLMed Al12Si is four times that of the sand-cast alloy which they attributed to the fine microstructure, but no detailed investigation of the strengthening mechanism(s) was reported. The lack of detailed investigation of the strengthening mechanism(s) is associated with the difficulty of observing dislocation movement in a fine microstructure during deformation. Recently, in-situ mechanical testing in the TEM has been performed in various materials [12-14] and live videos of dislocation movement can be recorded together with load-displacement information simultaneously. In the current work, the roles of cell boundaries and Si particles within the cells on the strength of laser fabricated samples have been studied by examining the dislocation structure in deformed samples and by carrying out in situ compression tests in a TEM.

Before presenting the results the terminology, which will be used throughout this paper, requires some clarification, because it is clear that different authors have used “cells” to describe different microstructures. The terminology used here will follow that used to describe the microstructures developed during solidification of alloys at different cooling rates, e.g. [15]. During slow cooling from the melt, dendrites are formed, which can form secondary and higher order dendritic arms to produce the well-known fern-like structure common in cast alloys, but at higher cooling rates there is no time for secondary dendrite arms to form and “cells” are formed instead. These are dendrites with effectively no secondary arms (very short secondary arms may well be formed)

that grow into the liquid, forming an array of parallel cells of the same orientation if they originate from the same nucleus. These cells may contain a substructure and in the present work the term “sub-cells” or simply “substructure” will be used to distinguish such features from the long cells. Grain boundaries are formed when columnar grains, growing from different nuclei meet.

2 Experimental

The powder used and the details of the powder bed technique used to produce samples have been described earlier [5] and will not be repeated here although the composition of the powder is shown in table 1.

Table 1. Chemical composition of the Al-10Si-0.4Mg alloy used in this study (wt.%).

Si	Mg	Ni	Ti	Mn	Zn	Fe	Pb	Sn	Al
9.92	0.291	0.04	0.006	0.004	0.01	0.137	0.004	0.003	Bal.

All samples were built using a Concept Laser M2 system. An island laser-scan strategy, with a 1 mm shift in the laser scanning direction between each layer, was used. The samples were built using the optimum process parameters identified in an earlier study [5], following a parametric optimisation study.

Several methods of sample preparation were used. As-fabricated bulk samples were mechanically polished and etched using Keller’s solution for SEM examination. As-fabricated XY section samples were prepared for TEM using electropolishing with a solution of 10%

perchloric acid and 90% methanol followed by Precision Ion Polishing system (PIPs). PIP was used because the electropolishing led to the deposition of silica on the sample surfaces and PIP reduced the extent of this contamination. In situ test samples were prepared by a Quanta 3D FEG Focussed Ion Beam (FIB), with a typical dimension of 400nm (thickness) × 1000nm (width) × 1000 nm (length).

SEM using secondary electron imaging, backscattered electron imaging and EBSD was carried out in a TESCAN MIRA-3. TEM examination was carried out in a JEOL 2100 microscope operating at 200kV. Two methods of obtaining diffraction information have been used; microdiffraction so that the region giving rise to the diffraction pattern was accurately defined by the focussed probe and selected area diffraction, using an aperture to define the selected area together with a defocussed electron beam, when a higher angular resolution was required [16]. Imaging of dislocations in these thinned samples was generally carried out using two-beam imaging conditions [16]. X-ray mapping was carried out on a TALOS STEM/TEM operating at 200kV. In some cases the same areas were examined by microdiffraction in the TEM and transmission Kikuchi diffraction (TKD) in the SEM so that direct comparisons could be made of the microstructures.

In-situ TEM compressions have been carried out on as-fabricated samples so that the behaviour of dislocations during compression can be directly observed. The in-situ tests used a Hysitron PI95 system, which was installed in a JEOL 2100 TEM. Rectangular cross section thinned samples are deformed by a flat probe so that they are subjected to strain in compression. The force, displacement and the video are recorded at the same time. The speed of the probe

deforming the sample was about 0.25 nm/s. Tensile tests were carried out at room temperature and sections from deformed samples examined using TEM in order to understand the role of cell boundaries, sub-cell boundaries and grain boundaries on dislocation path length.

3 Results.

3.1 Observations on YZ sections.

Examples of an EBSD image, a secondary electron image, and a back-scattered image of the same area of a YZ section of SLMed Al10Si0.4Mg are shown in figure 1. The EBSD image in figure 1(a) shows that the microstructure consists mostly of columnar grains, which can be up to hundreds of microns long and up to about 20μm in width, but there are some regions of equiaxed grains; the present paper focuses on the columnar grains, which dominate the microstructure. As reported earlier, e.g. [11], the columnar grains contain a cell-like sub-structure typically on the scale of about 500nm, with boundaries of Si rich-regions, as can be seen in figure 1(b). These sub-cells tend to be elongated in the Z-direction as is clear in figure 1(b). Comparison between figures 1(a), (b) and (c) shows that it is not easy to detect the grain boundaries between the columnar grains on the secondary image in figure 1(b) or on the back scattered image in figure 1(c) although these are obvious in figure 1(a). Sub-cell boundaries, cell boundaries and grain boundaries are visible in figure 1(b), but are not easily distinguished because Al-Si eutectic is present in all boundaries.

Measurements of the volume fraction of Al-Si have been carried out on the secondary electron images obtained in SEM. These measurements suggest that there is about 35vol% of Al-Si in cell, sub cell and grain boundaries in the as-fabricated samples.

Figure 1 HERE

TEM images of a YZ section are shown in figure 2 where it can be seen that as expected there are long Al cells. Adjacent cells have virtually identical orientations until a grain boundary is reached. The cells, which are dark in figure 2(a), are all within one Al grain. These cells contain sub-cell boundaries along their length, which correspond to those in figure 1(b). EDX shows all boundaries are rich in Si.

The dark field image taken using an Al 200 reflection, shown in figure 2 (b) of the region indicated in figure 2(a) shows that the sub cells and the Al in the sub cell boundaries, show similar contrast suggesting they are of similar orientation. The diffraction patterns taken from a similar area are shown in figures 2(c), (d), (e) and (f), where the microdiffraction patterns ((c), (d) and (e) were taken from cells either side and within a cell boundary showing that the orientations are identical. The selected area pattern, (f), was taken so that the aperture covered the two cells and the cell boundary and no extra Al reflections are visible. These observations confirm that the sub-cells and the Al in the sub-cell boundaries have identical orientations. This orientation is constant along the length of the long cells and between parallel cells, despite the substructure within the long cells. At grain boundaries the orientation of cells changes, but unless diffraction data is used it is not obvious where grain boundaries are present because the Si-Al region is present at cell boundaries, sub-cell boundaries and at grain boundaries.

The diffraction patterns and images in figure 2 suggest that epitaxial growth of the Al continues through sub-cell boundaries. Thus the Al in the boundary has the same orientation as the Al in the long cell below and the Al, which solidifies above the boundary, has the same orientation as the Al in the boundary.

The typical width of individual long cells, which are separated by Si-rich boundaries, is about 500nm whereas the Al grains (defined by the areas for which the orientations of the Al cells is constant, as measured by microdiffraction and defined in EBSD images) are typically between 3 and 5μm in cross section, but as is apparent from figure 1(a) they can be up to at least 20 μm.

It should be noted that small Si particles, within some regions of the Al-Si boundaries are visible in the dark field image in figure 2(b), which suggests that a Si diffraction maximum was also within the objective aperture, although it was not obvious on the microdiffraction pattern. This would be reasonable since the spacing of the planes used for the dark field image, the {200} in Al, is close to that of the {220} in Si and if for these particles these two sets of planes were parallel the two beams would both pass through the objective aperture. The relation between the Al and the Si in the cell boundaries, sub cell boundaries and grain boundaries is returned to in the following section where XY cross sections are examined.

Figure 2 HERE

3.2 Observations on XY sections of as-fabricated samples

SEM images of an XY section are shown in figure 3, which are identical to those reported earlier (e.g. in [11]) of a cell-like sub-structure, varying in size from about 300 to 700nm, which EDX

on thin foils showed the cells were separated by Si-rich boundaries. These two regions, the Al and the Al-Si, are clearly cross sections of the structures seen in YZ sections.

These Al cells apparently contain a significant amount of Si (about 2% Si), but the Si signal was always accompanied by a significant oxygen count so that part of the Si signal comes from silica left from electro-polishing. As reported earlier (e.g [11]), it is clear from the secondary electron image that these cross sections of cells can vary in size quite significantly, from region to region and within any given region, which presumably reflect either local changes in thermal history or changes in the direction of the section with respect to the length of the columnar grains [11].

Figure 3 HERE.

Typical bright field TEM images and diffraction patterns taken from an XY section are shown in figure 4 and the microstructure shows cell-like structures, which are clearly cross sections of cells and the Al-Si boundaries between them. All regions within the dark area shown in figure 4 (a) have orientations within about 2° and as is clear from the diffraction pattern in (c) these are close to the Bragg condition for the reflection shown. On the other hand the regions showing bright contrast in (b) are imaged under conditions where no low order reflection is strongly excited i.e. under kinematic conditions as shown in (d).

Figure 4 HERE

The sensitivity of the level of contrast to the diffraction conditions is expected when using diffraction contrast [16] but in addition there are some small particles within the Al grains, as can be seen in figure 5, which contribute to the dark contrast when close to the Bragg condition. Stereo-microscopy shows that many of these are on the surface of the sample, but a significant number are within the foil.

Figure 5. HERE.

A typical STEM HAADF image and the corresponding X-ray map for Al and Si are shown in figure 6 (a) and (b), which show very clearly that the boundaries of the cell-like regions are rich in silicon

Figure 6 HERE

Further detailed observations have been carried out in order to define the nature of the Al-Si in boundaries. Thus selected area diffraction patterns, from the region arrowed in figure 7(a) that EDX showed was very high in Si, show ring patterns from Si within which there are some weak diffraction maxima as shown in figure 7(b). Dark field images using the arrowed maxima are shown in figure 7(c) and (d). From these diffraction patterns and images it is clear that the Si particles in the boundaries are randomly oriented and thus that only a few are visible when a diffraction maximum is used to form a dark field image.

Figure 7 HERE

It is very tedious to define the sizes of areas that have the same orientations using micro-diffraction in TEM, since this requires diffraction patterns to be recorded within each individual cell-like region, but once obtained this data can then be used to define the grain size of the Al since a different diffraction pattern will be visible when a grain boundary is located. The transmission Kikuchi diffraction (TKD) available on modern SEMs allows simultaneous collection of virtually all the signals required to characterise the microstructure. Typical images are shown in figures 8 which were taken from the area shown in figure 4 so that direct comparisons can be made.

Figure 8 HERE

The grain boundary, which exists between these different grains in figure 8(b) is not distinguishable from a cell boundary when simply imaged in TEM, as is evident from figure 8(c)

and diffraction data or orientation imaging is necessary in order to identify grain boundaries which define the extent over which the Al cells have identical orientations. Individual Kikuchi maps can of course be extracted from the orientation images shown in these figures and local orientations accurately defined.

3.3 TEM analysis of defects in deformed samples.

(i) XY Sections from samples failed in Tension. Samples, which were tested to failure in tension, have been examined in the TEM in order to assess the dislocation density. Imaging of these samples was very difficult partly because of the presence of silica on the foil surface and the strain contrast within the cells when imaged close to a Bragg condition. A many beam image of dislocations within such a sample is shown in figure 9 and it is clear that there is a high density of dislocations in the sample despite the fact that the plastic strain before fracture is less than 2%. The dislocation density is particularly high near the Al-Si-eutectic boundary.

Figure 9 HERE.

(ii) In situ TEM compression tests. Figure 10a shows a bi-grain pillar from an XY section of the as-fabricated sample, where the grain boundary is indicated by the white dashed line. Several cell boundaries are observed. The cell boundaries appear to vary in width depending on the amount of Si present or on the plane of the boundary. The pillar was compressed inside the TEM and the load-displacement curve is shown in figure 10b. The movie is available in the supplementary section. Some frames, corresponding to images taken at the arrowed stress levels, c, d and e in figure 10b are displayed in figure 10c-e. They show a single cell imaged under two-beam conditions, from the area indicated by the red box in figure 10a. Many Si particles in the cell centre are indicated by yellow arrows in figure 10c. As the load was increased, many

dislocations, indicated by red arrows in figure 10d, are observed to be pinned by the particles. Figure 10e shows a higher density of dislocations. Detailed examination of the movie shows the dislocations generated at the contact area of the sample and probe at low strains are localised in the cell. No obvious penetration through the cell boundaries is observed. When the force is increased, some dislocations are transmitted through the thin cell boundary, where the Si particles are discrete. After the whole compression, no obvious signs of significant transmission of dislocations through the thick cell boundaries are observed.

Figure 10 HERE

Figure 11a shows a TEM bright field image of a bi-grain pillar, where the white dashed line indicates a grain boundary. The cell boundary in the left grain varies in width and/or orientation along its length. The force-displacement curve of the in-situ TEM compression is shown in figure 11b. The arrows indicate where frames are taken from the video and displayed in figure 11c-f. At the beginning of the deformation, many dislocations are found in the sample (figure 11c). As the force is increased, the area in contact with the probe starts to deform (figure 11d). The red arrow indicates the slip direction and a small slip step can be observed in the end. The central region is not deformed at this stage, as indicated by the yellow arrows, the dislocations remain the same. Figure 11e shows the bottom region starts to deform, the slip direction is same as in the front part of figure 11d. The deformation is mostly localised in the front and the bottom part of the sample, where the cell boundary is thin. This is seen more clearly in the supplementary video 2. As shown in figure 11f, the central region is narrower than other parts, which also indicates the strains are smaller.

Figure 11 HERE

4 Discussion

The observations reported in this paper cover two areas, which will be discussed in turn; firstly, the microstructure of as fabricated samples and secondly, the role of the Si particles within cells and of Al-Si boundaries in limiting dislocation path length.

The first aim of this paper is the characterisation of the microstructure of as-fabricated samples using TEM, STEM and SEM for both XY and YZ sections, with the aim of understanding the origin of the complex structures reported in the present work and in several recent papers. As noted earlier it is essential to distinguish between three types of "cell-like" structures; (i) long "cells" which are formed instead of dendrites because of the cooling conditions [15] (ii) cell-like structures which are seen (in XY sections) because they are cross sections of the long cells in the build direction and (iii) the substructure consisting of slightly elongated sub-cells found in YZ sections within the length of the long cells.

The present observations can be understood if Al cells, (with a limited amount of Si in solution) are the first phase to solidify leaving liquid of approximately eutectic composition between them. Subsequently this liquid solidifies and forms Si-Al eutectic to produce long cell boundaries in YZ sections, separated by eutectic, as expected during cell growth [15]. Adjacent regions of cells, growing from a nucleus of a different orientation are separated by Al grain boundaries, which also contain Al-Si eutectic but these grain boundaries are not easily distinguished from cell boundaries in the absence of diffraction data. Thus in secondary electron images from a YZ section such as that shown in figure 1(b) it appears that the only boundaries which are present are those between the long cells and those within these long cells. Although grain boundaries are

present they cannot be identified from such images. As noted earlier comparison between figure 1(a), the EBSD image and figures 1(b) and (c), allows identification of grain boundaries.

In an XY section the cross sections of these cells would generally appear to be "cell-like features" having the same orientation within each individual parent Al columnar grain, since the XY section usually cuts across the lengths of these cells. They are separated by cross sections of the Si-rich eutectic present between the cells. These cross sections of long cells would also be expected to contain Al-Si eutectic in the sub-cell boundaries, visible in figure 1(b) and Si precipitates within the cells, as in figure 5.

The observation that within the Al cells visible in YZ sections there are also cell-like features (see figure 1) which have boundaries consisting of Al-Si eutectic, has also been reported by other workers including Thijs et al [11]. In their paper they refer to these features as "cells" varying in size from less than a micron to a few microns. They suggest that this structure is formed directly by solidification taking place as "cellular dendrites" caused by the high cooling rate during SLM, but no detailed mechanism is suggested for their formation. Li et al. [6] have suggested that these Si-rich boundaries separate Al grains and Aboulkhair et al. [10] suggest that the structure in XY sections is a fine eutectic made up of Al grains and Si. In addition to these differing interpretations of the microstructures observed in different sections of SLMed samples it has also been suggested that the structure consists of Al and Si dendrites [7, 17]. The origin and nature of microstructures, which appear to be identical, have thus been interpreted in many different ways.

The suggestion that Al cells are formed first is clearly capable of explaining the presence of Al-

Si eutectic between the long cells. The additional observation that has to be understood is the mechanism whereby individual long cells can be formed which have a constant orientation over several tens or hundreds of microns, despite the fact that they contain regions of Al-Si eutectic perpendicular to the growth direction (and in all other directions) spaced at distances of a few hundred nanometres, which form a substructure within the long cells. This eutectic could, but does not, provide discontinuities in the growth of the long Al cells. If the mechanism of cell growth postulated here is correct, the Al-Si eutectic within the cells must be formed under conditions that allow epitaxy between the Al in the cells and the Al in the eutectic during solidification. This eutectic liquid is formed as Al solidifies and if some is left on the surface of the solid Al as it solidifies it will be incorporated into the long cells as growth continues. The experimental observations reported in figure 2 in fact show that the Al in the eutectic formed within cells has the same orientation as that in the Al immediately below and immediately above, so that the Al in the eutectic grows epitaxially on the pre-existing Al and subsequent growth of the Al cell in the Z-direction continues epitaxially on the Al in the eutectic. Because there is such a high fraction of eutectic in this alloy in as fabricated samples it is not unexpected that eutectic liquid as well as forming between cells is also left on the surface of the growing cells which then produces the substructure of sub cells visible in the secondary images and TEM images taken from YZ sections.

The observations in figure 7 are typical of those found in this study where both weak ring patterns and weak individual diffraction maxima from the Si in the eutectic in cell boundaries could be observed from regions high in Si; from regions lower in Si these diffraction maxima were generally too weak to be seen in microdiffraction patterns but are visible in selected area

patterns, because of the superior angular resolution. The random orientation of the Si precipitates suggests that no orientation relationship between the Al and Si exists although as would be expected there were occasions, such as that shown in figure 2 where the {200} in Al are parallel with the {220} in Si in some grains. This contrasts with the conclusion drawn by Li et al [6], where they suggest that there is an orientation relationship with the {111} in Si parallel to the {200} in Al. It is perfectly reasonable to expect that sets of planes in the two crystals are occasionally parallel (as in the pattern shown in figure 2 (b), but this does not imply an orientation relationship. With such a large misfit between the 3.13Å spacing of the {111} in Si and the 2.024Å spacing of the {002} in Al it is not obvious why such an orientation relationship should exist. The fact that the particles tend to be spherical, that ring patterns are observed and that only a few of them are imaged when using a specific Si reflection are all further evidence that there is no obvious orientation relationship between the Al and the Si and that the particles of Si in the eutectic have a random orientation.

The second aim was to understand the origin of the high strength of laser-fabricated samples. The observations of dislocations in as-fabricated polycrystalline samples deformed in tension showed very high dislocation densities, but detailed analysis was not possible because of specimen preparation difficulties. Nevertheless it is reasonable to conclude that the high dislocation density reflects the fact that the Si within the cells and the Al-Si-eutectic boundaries limit the path length of dislocations. This was confirmed directly by the in situ observations where it is clear on the movie that the moving dislocations interact both with the Si within the cells and with the cell boundaries (and grain boundaries) which block the movement of dislocations. It seems reasonable to conclude as suggested earlier (e.g. [6, 11]) that the high

strength of the as-fabricated samples is caused by the fineness of the structure defined by the Al-Si eutectic and the Si particles within cells. In fact in some, but not in all earlier work, the as-fabricated samples had higher yield strengths than fully heat-treated samples.

5. Conclusions

1 Microdiffraction in TEM at a spatial resolution of 10's of nms is essential if the microstructures of as-fabricated SLM samples are to be characterised.

2 Long cells are formed because of the high cooling rate and boundaries between the cells form from eutectic liquid that is rejected as the Al cells solidify.

3 The cell-like structures, seen in sections perpendicular to the build direction of SLMed samples are cross sections of identical orientation long cells. Adjacent cells thus have virtually the same orientation until a grain boundary is crossed.

4 These long cells maintain their orientations during growth, despite the substructure of Al-Si eutectic boundaries within the length of the cells, because the Al within the eutectic grows epitaxially on the pre-existing Al cell, which in turn gives rise to further epitaxial growth of the Al cell, which is formed above the eutectic.

5 The strength of As-F SLMed Al-10Si-0.4Mg is high because the Al grains contain regions of about 500nm diameter, that contain Si particles and which are surrounded by 10-20nm thick eutectic, which inhibits dislocation motion within the larger Al grains.

6 The heterogeneous microstructure, varying between columnar and equiaxed would be expected to lead to local differences in strength if the distribution of the Si particles and the Al-Si eutectic is different in different regions, which presents a challenge to this technology if critical components are to be produced.

Acknowledgements

Discussions with many colleagues, during the formulation of the ideas in this paper, are gratefully acknowledged. Financial support from Paul Bowen, Head of Metallurgy and Materials is also acknowledged.

References

[1] H. Ye, An overview of the development of Al-Si-Alloy based material for engine applications, J. Mater. Eng. Perform. 12 (2003) 288-297.

[2] B. Li, H. Wang, J. Jie, Z. Wei, Effects of yttrium and heat treatment on the microstructure and tensile properties of Al-7.5Si-0.5Mg alloy, Mater. Design 32 (2011) 1617-1622.

[3] C.H. Cáceres, C.J. Davidson, J.R. Griffiths, The deformation and fracture behaviour of an Al-Si-Mg casting alloy, Mater. Sci. Eng. A 197 (1995) 171-179.

[4] D.D. Gu, W. Meiners, K. Wissenbach, R. Poprawe, Laser additive manufacturing of metallic components: materials, processes and mechanisms, Inter. Mater. Rev. 57 (2012) 133-164.

[5] N. Read, W. Wang, K. Essa, M.M. Attallah, Selective laser melting of AlSi10Mg alloy: Process optimisation and mechanical properties development, Mater. Design 65 (2015) 417-424.

[6] X.P. Li, X.J. Wang, M. Saunders, A. Suvorova, L.C. Zhang, Y.J. Liu, M.H. Fang, Z.H. Huang, T.B. Sercombe, A selective laser melting and solution heat treatment refined Al–12Si alloy with a controllable ultrafine eutectic microstructure and 25% tensile ductility, Acta Mater. 95 (2015) 74-82.

[7] S. Siddique, M. Imran, E. Wycisk, C. Emmelmann, F. Walther, Influence of process-induced microstructure and imperfections on mechanical properties of AlSi12 processed by selective laser melting, J. Mater. Process. Tech. 221 (2015) 205-213.

[8] T. Vilaro, V. Kottman-Rexerodt, M. Thomas, C. Colin, P. Bertrand, L. Thivillon, S. Abed, V. Ji, P. Aubry, P. Peyre, Direct fabrication of a Ti-47Al-2Cr-2Nb alloy by selective laser melting and direct metal deposition processes, Adv. Mater. Res. 89-91 (2010) 586-591.

[9] E. Brandl, U. Heckenberger, V. Holzinger, D. Buchbinder, Additive manufactured AlSi10Mg samples using Selective Laser Melting (SLM): Microstructure, high cycle fatigue, and fracture behavior, Mater. Design 34 (2012) 159-169.

[10] N.T. Aboulkhair, C. Tuck, I. Ashcroft, I. Maskery, N.M. Everitt, On the Precipitation Hardening of Selective Laser Melted AlSi10Mg, Metall. Mater. Trans. A 46 (2015) 3337-3341.

[11] L. Thijs, K. Kempen, J.-P. Kruth, J. Van Humbeeck, Fine-structured aluminium products with controllable texture by selective laser melting of pre-alloyed AlSi10Mg powder, Acta Mater. 61 (2013) 1809-1819.

[12] S.H. Oh, M. Legros, D. Kiener, G. Dehm, In situ observation of dislocation nucleation and escape in a submicrometre aluminium single crystal, Nat. Mater. 8 (2009) 95-100.

[13] J. Ye, R.K. Mishra, A.K. Sachdev, A.M. Minor, In situ TEM compression testing of Mg and Mg-0.2 wt.% Ce single crystals, Scripta Mater. 64 (2011) 292-295.

[14] Z.W. Shan, J. Li, Y.Q. Cheng, A.M. Minor, S.A. Syed Asif, O.L. Warren, E. Ma, Plastic flow and failure resistance of metallic glass: Insight from in situ compression of nanopillars, Phys. Rev. B, 77 (2008) 155419.

[15] W. Kurz, D.J. Fisher, Fundamentals of Solidification (3rd edition), Trans Tech Publications, 1992.

[16] P.B. Hirsch, A. Howie, R.B. Nicholson, D. Pashley, M.J. Whelan, Electron Microscopy of Thin Crystals, Butterworths, 1965.

[17] L.A. Jacobson, J. McKittrick, Rapid solidification processing, Mater. Sci. Eng. R 11 (1994) 355-408.

Figure 1

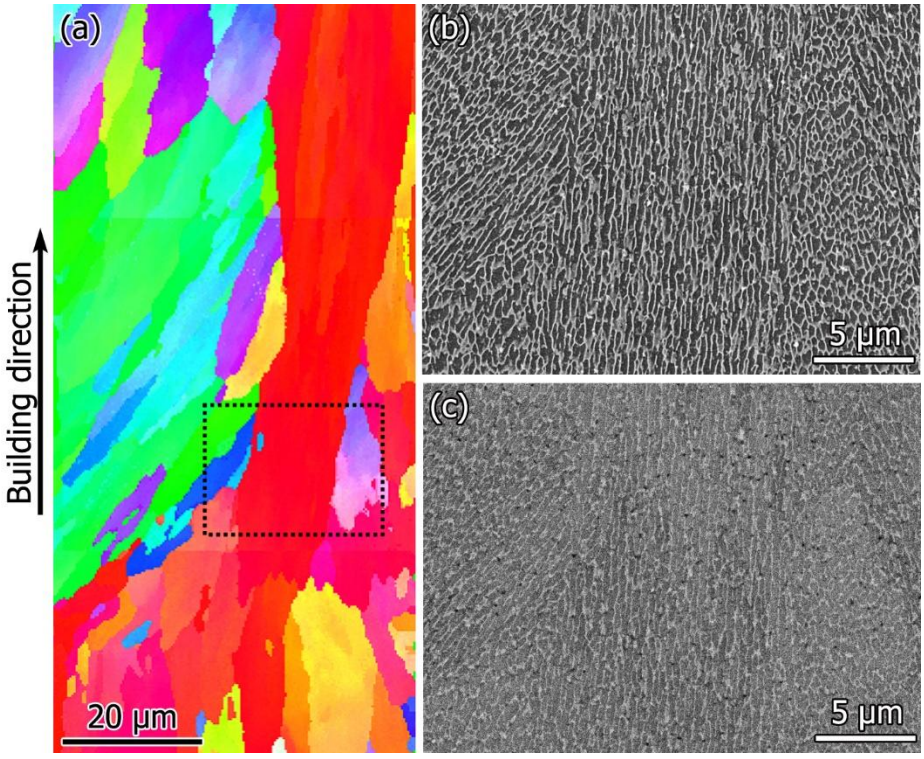

Figure 1 SEM images of a YZ section of an as fabricated sample of Al-10Si-0.4Mg: (a) EBSD; (b) secondary electron; (c) back scattered. The dashed rectangle in (a) shows the area from which the secondary and back-scattered images were obtained.

Figure 2

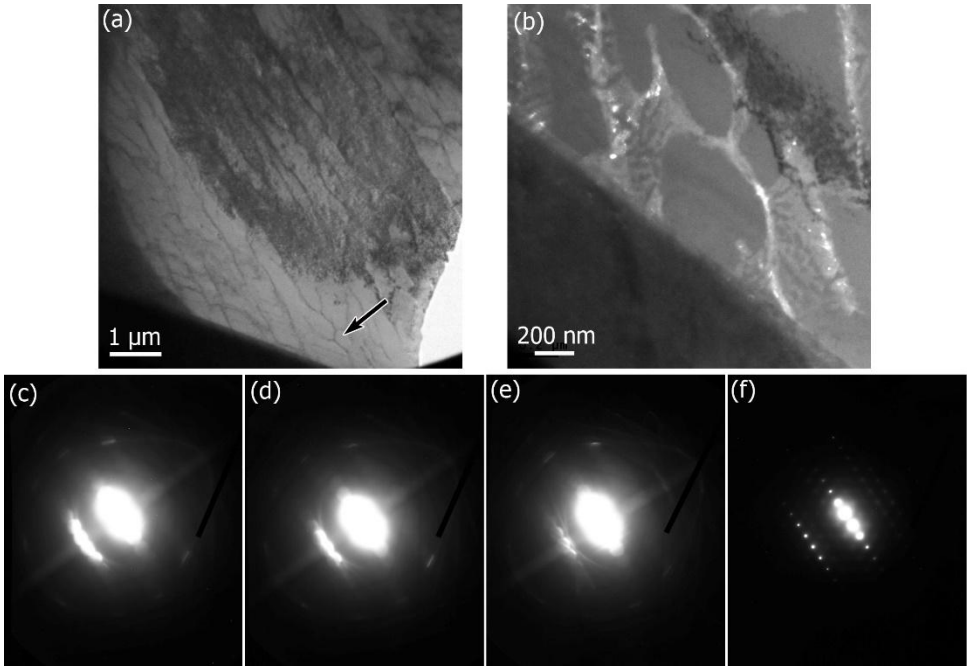

Figure 2 (a) Bright field and (b) dark field TEM image taken using an Al-reflection. The dark field image shows similar intensity contrast in the cell boundaries and cell centres. The arrow indicates the region from which (b) was obtained. The microdiffraction pattern, (c), (d) and (e) were taken from cells either side of a cell boundary and directly on the cell boundary. The selected area pattern, (f), was taken covering the two cells and the cell boundary. These four patterns show that the Al within the boundaries either side of the cells along the growth direction have identical orientations to the cells.

Figure 3

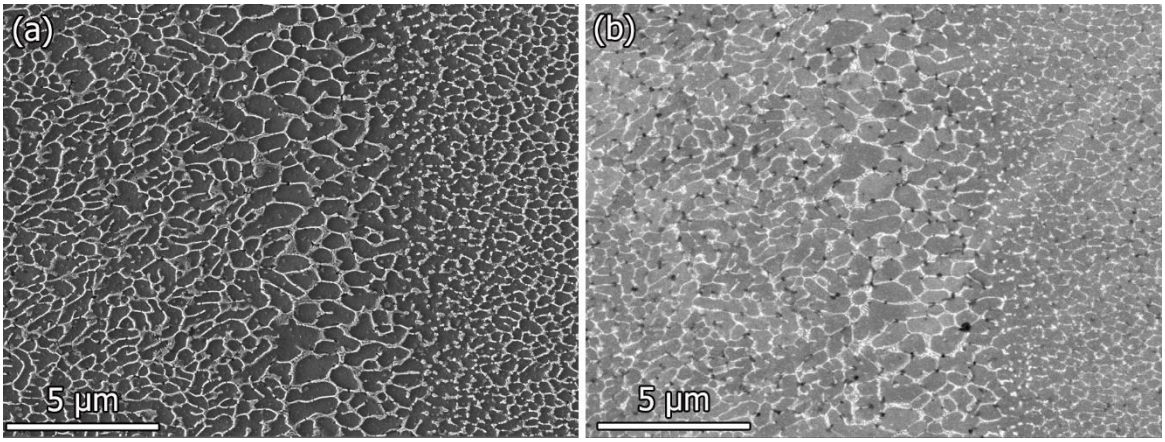

Figure 3 SEM images of an XY section of SLMed sample of Al-10Si-0.4Mg, showing sections of the cells in YZ sections; (a) secondary electron (b) back scattered.

Figure 4

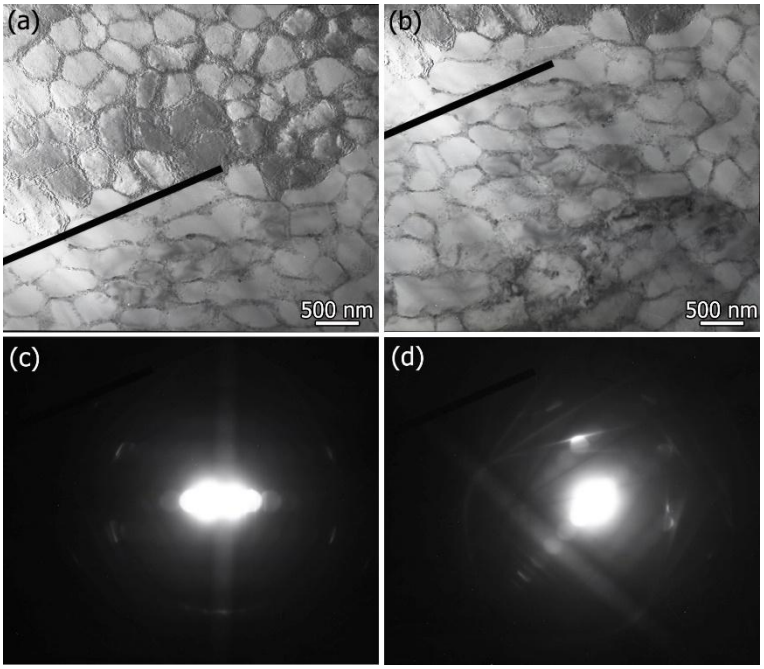

Figure 4 TEM images and diffraction patterns of an XY section of SLMed Al-10Si-0.4Mg. (a) and (b) bright field images and (c) and (d) corresponding diffraction patterns taken from the areas indicated by the pointer.

Figure 5

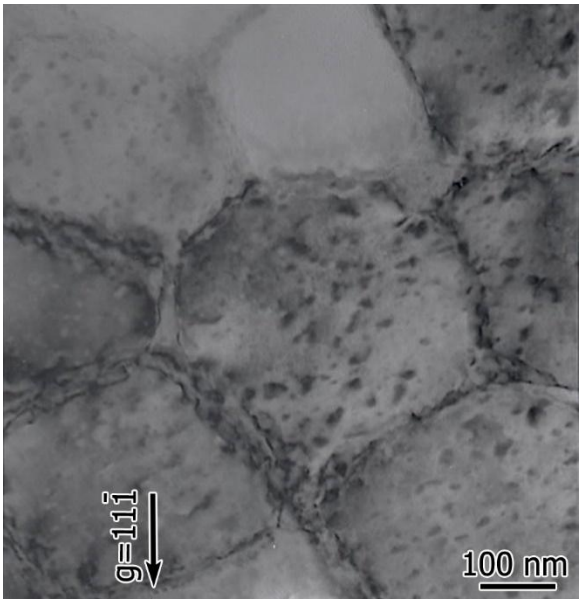

Figure 5. Bright field TEM image of XY section of an electropolished and PIPped as-fabricated sample of Al10Si0.4Mg. B = [123] with a 11-1 reflection (arrowed) close to Bragg.

Figure 6

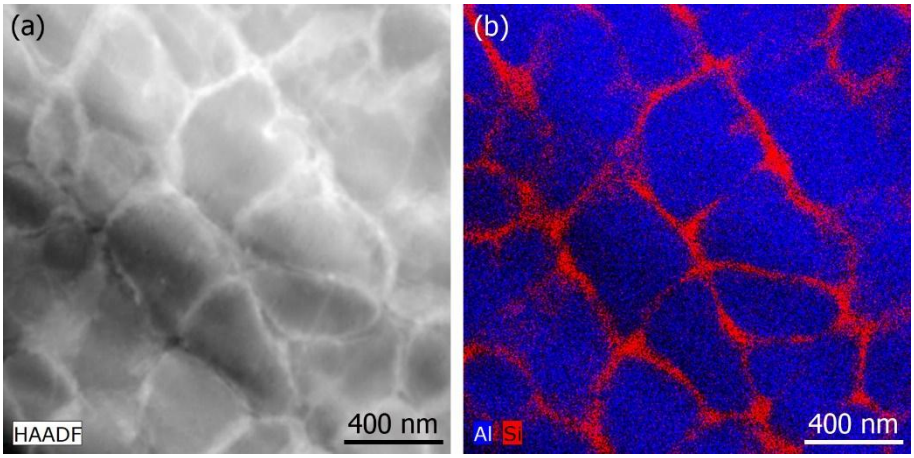

Figure 6 Images of an XY section of as-fabricated Al10Si0.4Mg: (a) STEM HAADF image; (b) Al and Si X-ray map.

Figure 7

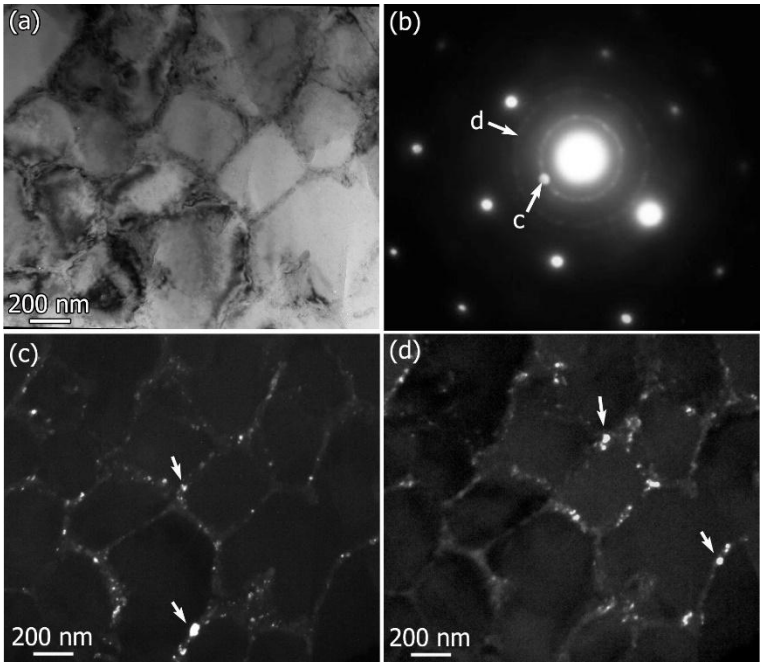

Figure 7 (a) A bright field image taken under many beam conditions of a region (arrowed) which EDX showed was very high in Si. (b) A selected area diffraction pattern taken from the arrowed region in (a). This pattern shows maxima from Al and indexed Si ring patterns and some weak maxima on these rings two of which (arrowed) were used to form the dark field images shown in (c) and (d).

Figure 8

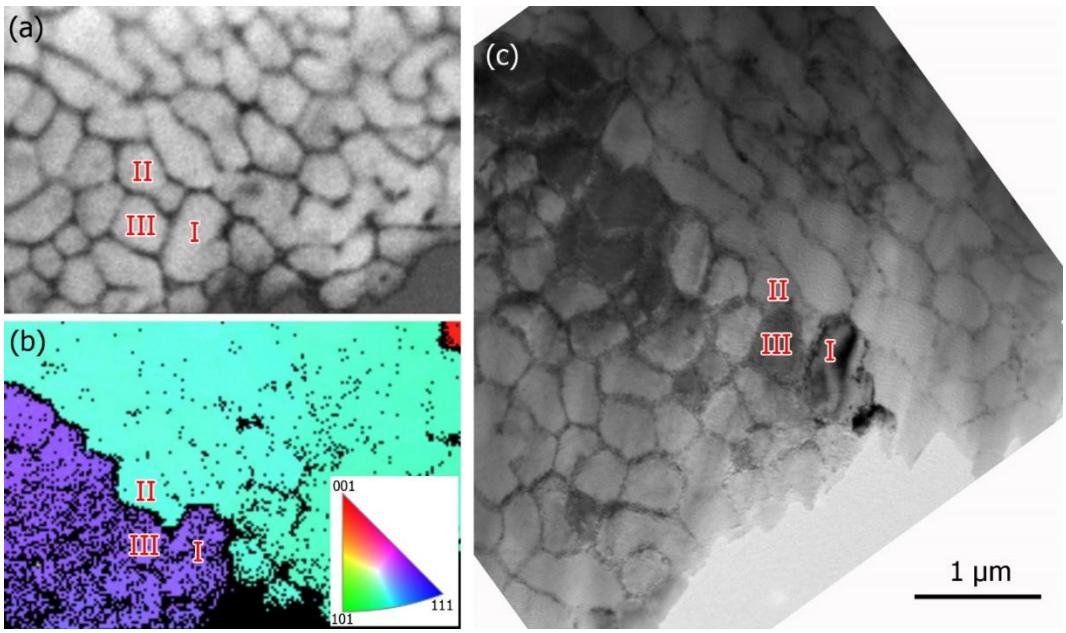

Figure 8 (a) TKD (Transmission Kikuchi Diffraction) band contrast image and (b) orientation map taken from the area from the area imaged in figure 4 showing the two Al grains each containing identical orientation "cell-like" structures. (c) TEM image of the same area.

Figure 9

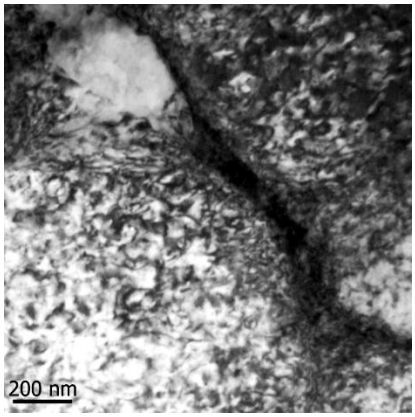

Figure 9 Many beam TEM image of an XY section of a sample of as fabricated Al-10Si-0.4Mg tested to failure in tension. A very high dislocation density is apparent, but the poor quality of the images that could be obtained (see text) precludes detailed analysis. The dark contrast at the cell boundary is associated with a very high dislocation density.

Figure 10

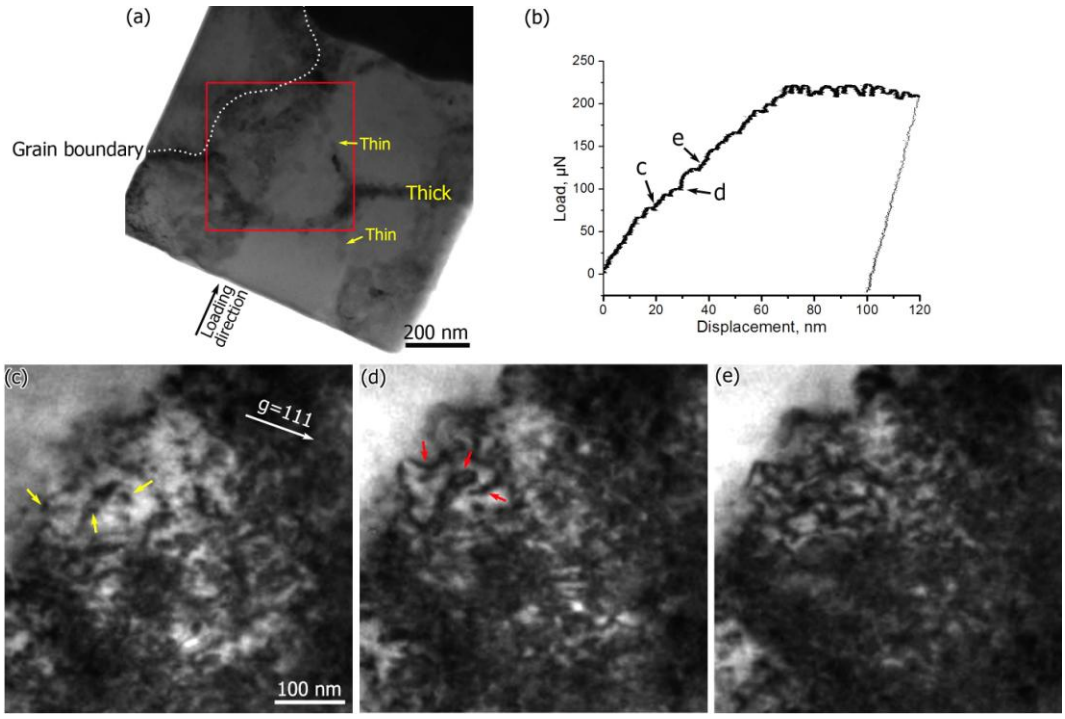

Figure 10 (a) TEM bright-field image of a bi-grain pillar before in-situ compression under many beam condition; (b) In-situ compression load-displacement; (c-e) TEM bright-field images under two beam condition corresponding to stress levels c and d in figure 9b. The images are magnified images of the rectangular area in figure 10a.

Figure 11

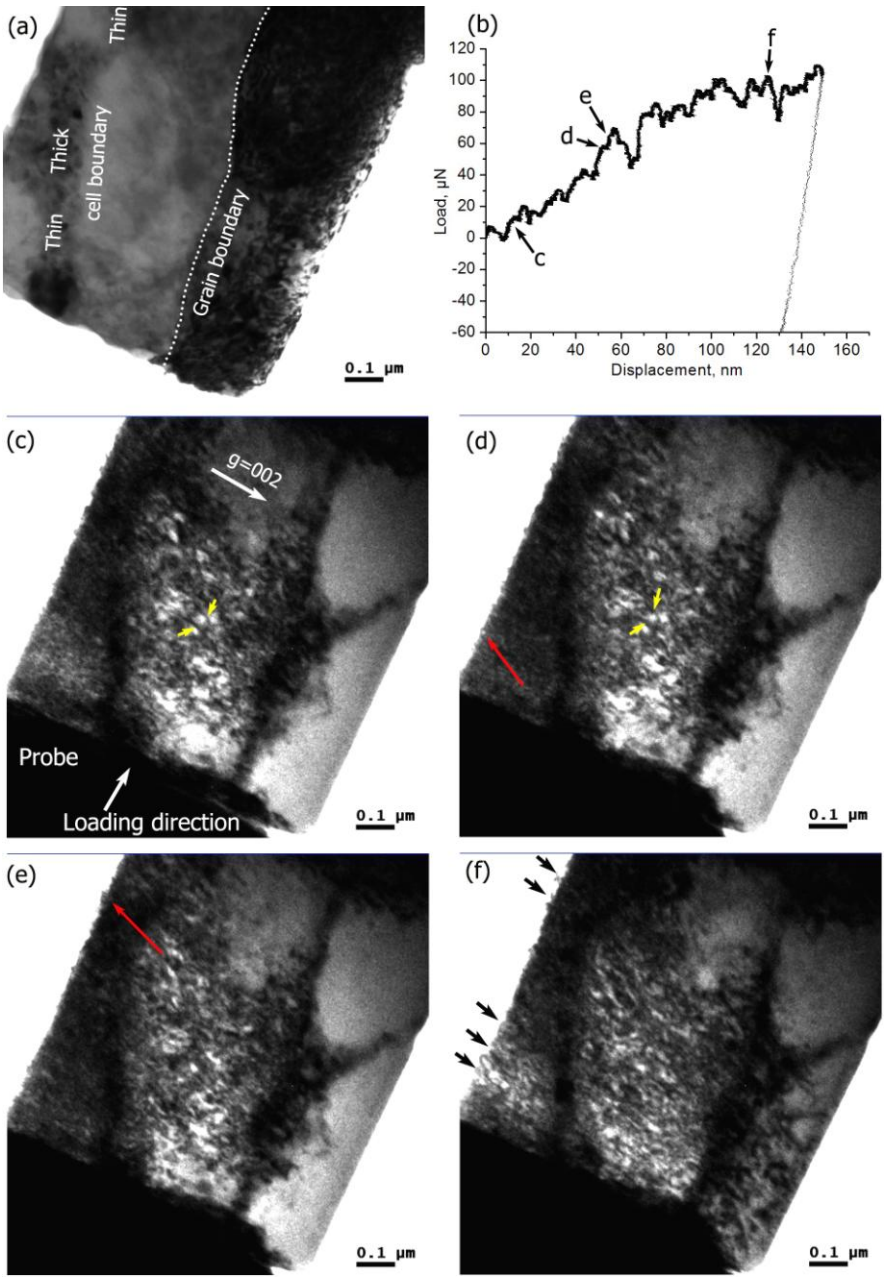

Figure 11 (a) TEM bright-field image of a bi-grain sample under many beam condition; (b) Load-displacement curve of the in-situ compression. The loading direction is indicated in the figure. After unloading the sample shows negative force, which is due to the tensile stress caused by attachment between the sample and probe; (c-f) Bright-field images corresponding to the load-displacement curve. The left grain is under two beam conditions where the dislocations can be seen. The right grain is under kinematic conditions.

Supplementary video 1

Click here to download Supplementary Material: Supplementary video 1.mp4

Supplementary video 2

Click here to download Supplementary Material: Supplementary video 2.mp4

*Graphical Abstract

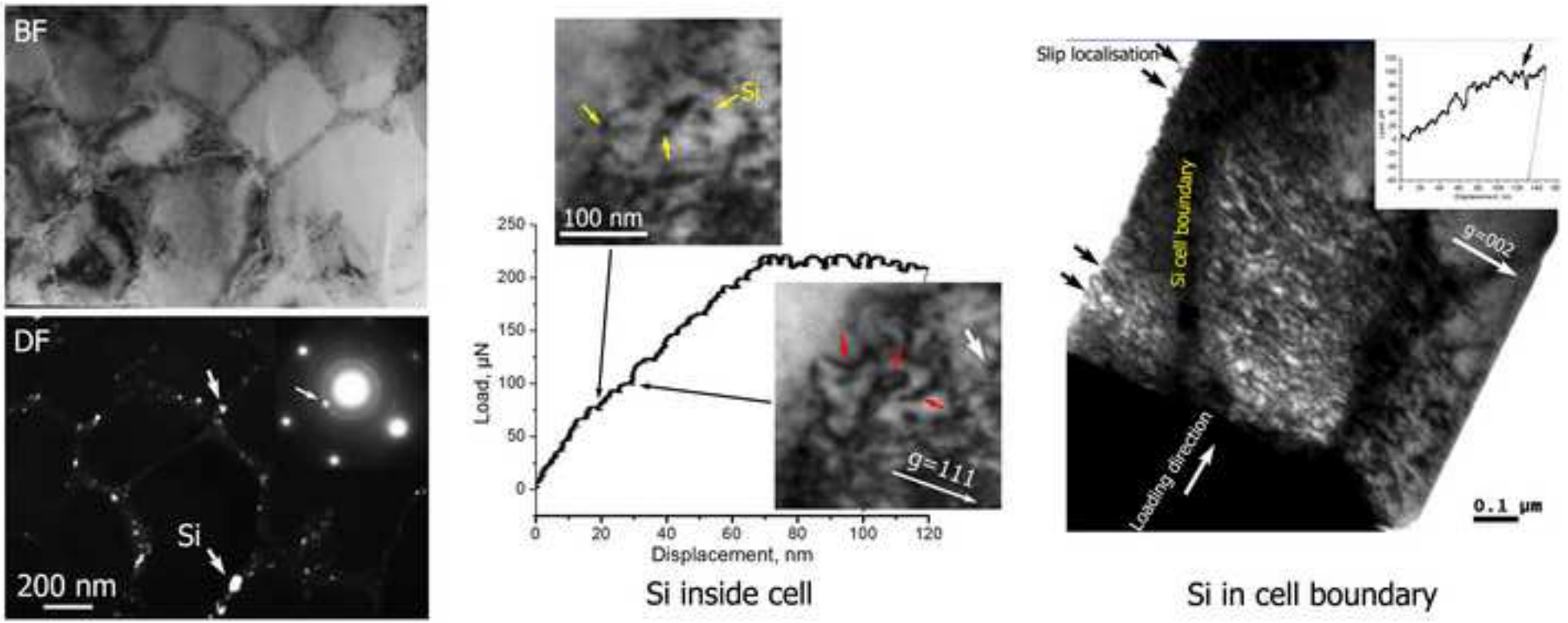

Si inside cell

Si in cell boundary